Cryogenics 64 (2014) 29–39

Contents lists available at ScienceDirect

Cryogenics

journal homepage: www.elsevier.com/locate/cryogenics

# Investigation of two-phase heat transfer coefficients of argon–freon cryogenic mixed refrigerants

Seungwhan Baek [a,*,2], Cheonkyu Lee [b,1], Sangkwon Jeong [b,1]

[a] Applied Chemicals and Materials Division 647, Material Measurement Laboratory, National Institute of Standards and Technology (NIST), 325 Broadway, Boulder, CO 80305, USA
[b] Cryogenic Engineering Laboratory, #5119, Department of Mechanical Engineering, Korea Advanced Institute of Science and Technology (KAIST), 291 Daehak-ro, Yuseong-gu, Daejeon 305-701, Republic of Korea

ARTICLE INFO

*Article history:*
Received 5 June 2014
Received in revised form 10 September 2014
Accepted 17 September 2014
Available online 28 September 2014

*Keywords:*
Mixed refrigerant
Two-phase
Evaporation
Condensation
Heat transfer coefficient
Microchannel

ABSTRACT

Mixed refrigerant Joule Thomson refrigerators are widely used in various kinds of cryogenic systems these days. Although heat transfer coefficient estimation for a multi-phase and multi-component fluid in the cryogenic temperature range is necessarily required in the heat exchanger design of mixed refrigerant Joule Thomson refrigerators, it has been rarely discussed so far. In this paper, condensation and evaporation heat transfer coefficients of argon–freon mixed refrigerant are measured in a microchannel heat exchanger. A Printed Circuit Heat Exchanger (PCHE) with 340 μm hydraulic diameter has been developed as a compact microchannel heat exchanger and utilized in the experiment. Several two-phase heat transfer coefficient correlations are examined to discuss the experimental measurement results. The result of this paper shows that cryogenic two-phase mixed refrigerant heat transfer coefficients can be estimated by conventional two-phase heat transfer coefficient correlations.



## 1. Introduction

As the demand for compact and efficient cryogenic Joule–Thomson refrigeration systems increases, two major technologies are being employed. Firstly, a microchannel configuration is often utilized in the heat exchanger of such refrigeration systems. The microchannel can increase the heat transfer area due to the small hydraulic diameter of the channel; the area density of the heat exchanger is increased within the same volume (compared to that of a conventional heat exchanger). Therefore, a compact and high effectiveness heat exchanger can be developed in the refrigeration system. Besides, the heat transfer coefficient is larger than that of the macrochannels due to its small hydraulic diameter; thus, the higher performance can be achieved within the same volume of heat exchanger. The second method to improve the efficiency of cryogenic refrigeration systems is to reduce the required work from the compressor. When a Joule–Thomson refrigerator with a single-component refrigerant is utilized to reach cryogenic temperatures, very high compression ratios are usually required, which results in high compression work. The zeotropic mixed refrigerant has been introduced to reduce the compression ratio and the energy consumption [1]. A mixed refrigerant Joule–Thomson refrigerator can have a higher cooling power than a single component refrigerant Joule–Thomson refrigerator at the identical compression ratio. The distinctive difference of the mixed refrigerant refrigeration process from the pure component refrigeration process is that the mixed refrigerant works almost completely in the two-phase region. Fig. 1 displays the temperature-entropy diagram of the pure substance argon and a mixed refrigerant. Use of a mixed refrigerant enlarges the vapor dome as compared to the vapor dome of a pure substance. Therefore, the mixed refrigerant at high pressure gets condensed during the cool down, while the low pressure stream from the evaporator gets evaporated in the heat exchanger. For this reason, the detailed information of the two-phase heat transfer coefficients are indispensable for the design of the recuperative heat exchanger for a mixed refrigerant Joule Thomson refrigerator.

There are several papers [2–4] related to the design of tube-in-tube heat exchangers for mixed refrigerant Joule–Thomson refrigerators. These heat exchangers were composed of macrochannels with 10–14.5 mm for the outer tube and 2 mm for the inner tubes. They analyzed only the overall heat transfer coefficients for the

* Corresponding author. Tel.: +1 303 497 4866; fax: +1 303 497 6682.
*E-mail addresses:* sbaek@nist.gov (S. Baek), cheonkyu_lee@kaist.ac.kr (C. Lee), skjeong@kaist.ac.kr (S. Jeong).
[1] Tel.: +82 42 350 3039; fax: +82 42 350 8207.
[2] Contributions of NIST, not subject to copyright in the United States.

http://dx.doi.org/10.1016/j.cryogenics.2014.09.004

**Nomenclature**

*Symbols*

| | |
|---|---|
| $A$ | heat transfer area, $m^2$ |
| $a$ | shear stress constant |
| AAD | absolute average deviation |
| $B$ | total bias error |
| $Bo$ | boiling number $(q''/(i_{lv}G))$ |
| $C_{lg}$ | correction factor, |
| $C_p$ | heat capacity, J/kg K |
| $C_{pw}$ | apparent local specific heat, J/kg K |
| $D_h$ | hydraulic diameter, m |
| $E$ | two-phase multiplier constant |
| $F$ | two-phase multiplier constant |
| $Fr$ | Froude number $(G^2/(gD\rho_{tp}^2))$ |
| $G$ | mass flux, $kg/m^2$ s |
| $g$ | gravitational acceleration, $m/s^2$ |
| $h$ | local heat transfer coefficient, $W/m^2$ K |
| $H$ | two-phase multiplier constant |
| $i$ | enthalpy, J/kg |
| $k$ | thermal conductivity, W/mK |
| $m$ | mass flow rate, kg/s |
| $M$ | molecular weight |
| $N$ | number of data |
| $Nu$ | Nusselt number |
| Pr | Prandtl number |
| $P_r$ | reduced pressure |
| $Q$ | heat flow, W |
| $q''$ | heat flux, $W/m^2$ |
| $R$ | two-phase multiplier constant |
| $Re$ | Reynolds number |
| $S$ | standard deviation of data |
| $S$ | two-phase multiplier constant |
| $T$ | temperature, K |
| $t_{95\%}$ | T-distribution for a confidence level |
| $U$ | overall heat transfer coefficient, $W/m^2$ K |
| $U$ | uncertainty |
| $We$ | Weber number $(G^2D/(\sigma\rho_{tp}))$ |
| $x$ | quality |
| $X_o$ | two-phase multiplier constant |
| $X_{tt}$ | Lockhart–Martinelli parameter |
| $Z$ | two-phase multiplier constant |
| $z$ | distance |

*Greek symbols*

| | |
|---|---|
| $\lambda$ | the ratio of interface velocity to mean film velocity |
| $\mu$ | viscosity, Pa s |
| $\rho$ | density, $kg/m^3$ |
| $\sigma$ | surface tension, N/m |
| $\tau$ | shear stress, Pa |

*Subscripts*

| | |
|---|---|
| *bc* | bulk convective contribution |
| *cond* | condensation |
| *eq* | equivalent |
| *evap* | evaporation |
| *exp* | experimental |
| *f* | shear stress due to friction |
| *He* | helium |
| *HT* | heat transfer area |
| *in* | inlet |
| *L* | total length |
| *l* | liquid |
| *LMTD* | log mean temperature difference |
| *lo* | liquid only |
| *lv* | differential of latent (vapor–liquid) |
| *m* | shear stress due to momentum |
| *MR* | mixed refrigerant |
| *nb* | nucleate pool boiling contribution |
| *out* | outlet |
| *pred* | prediction |
| *sat* | saturation |
| *tp* | two-phase |
| *v* | vapor |
| *vo* | vapor only |
| *w* | wall |

heat exchanger or the overall performance of the Joule Thomson refrigerator. The measurement of the overall heat transfer coefficient data does not allow investigation of the local heat transfer coefficients. Further development of heat exchangers for mixed refrigerant Joule–Thomson refrigerators requires local heat transfer coefficient measurements of two-phase mixed refrigerants. The local evaporative heat transfer coefficient of the two-phase mixed refrigerant was obtained by Nellis [5] for a circular channel ($D_h$ = 860 μm), and this is probably the only reported study on a multi-component mixture at cryogenic temperature. On the other hand, the condensation heat transfer coefficient of cryogenic mixed refrigerant has not been reported elsewhere.

Substantial work has been reported in conjunction with evaporation and condensation of room temperature mixed refrigerants. Cheng et al. [6] and Celata et al. [7] reviewed the evaporative heat transfer characteristics of mixed refrigerants. Radermacher and Hwang [8] summarized the research related to the condensation heat transfer mechanism of mixed refrigerants. However, these mixed refrigerants are composed of CFCs and HCFCs used for room temperature applications such as HVAC and electronics cooling devices. The temperature glide for these mixtures is usually less than 10 K and the variation in the physical properties is not significant compared to the cryogenic mixed refrigerants used in cryocoolers. The hydraulic diameter was larger than 7 mm the in preceding research.

For the design process of an appropriate microchannel heat exchanger for a mixed refrigerant Joule–Thomson refrigerator, local evaporation and condensation heat transfer coefficients of the mixed refrigerant should be identified. In this paper, two phase heat transfer coefficients for evaporation and condensation of argon–freon mixed refrigerants in the cryogenic temperature range are investigated by using a microchannel heat exchanger in the form of a Printed Circuit Heat Exchanger ($D_h$ = 340 μm). The Log Mean Temperature Difference (LMTD) heat exchanger analysis is utilized to find heat transfer coefficients. Nellis [5] investigated only the evaporation heat transfer coefficients of nitrogen-hydrocarbon mixtures using a directly applied electro-thermal heat load. The research in our paper study uses the counter flowing stream of helium as the heat load in the counterflow heat exchanger, which enables the measurement of the evaporation and also the condensation heat transfer coefficients. The measured data only indicates the temperature (or quality) averaged value, however, these obtained results can be useful to the design of the recuperator for the cryogenic mixed refrigerant Joule Thomson refrigerator. The measured heat transfer coefficients are compared with the previously developed correlations.

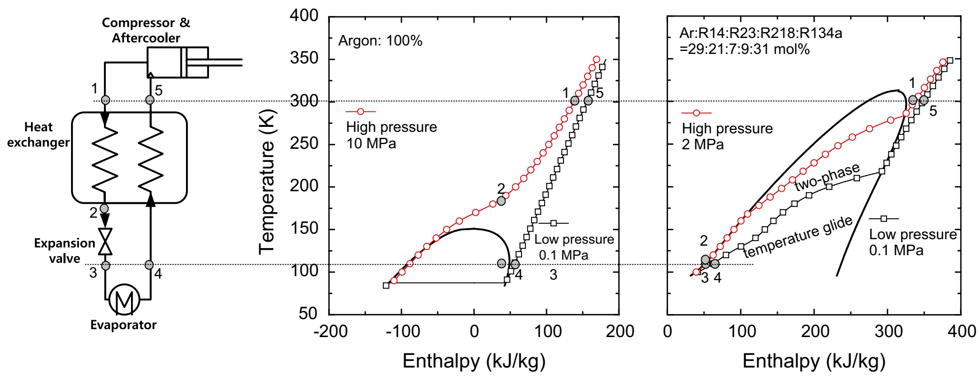


**Fig. 1.** The Joule Thomson cooling process with pure fluid (Ar) and mixed refrigerant (Ar:R14:R23:R218:R134a = 29:21:7:9:31 mol%).

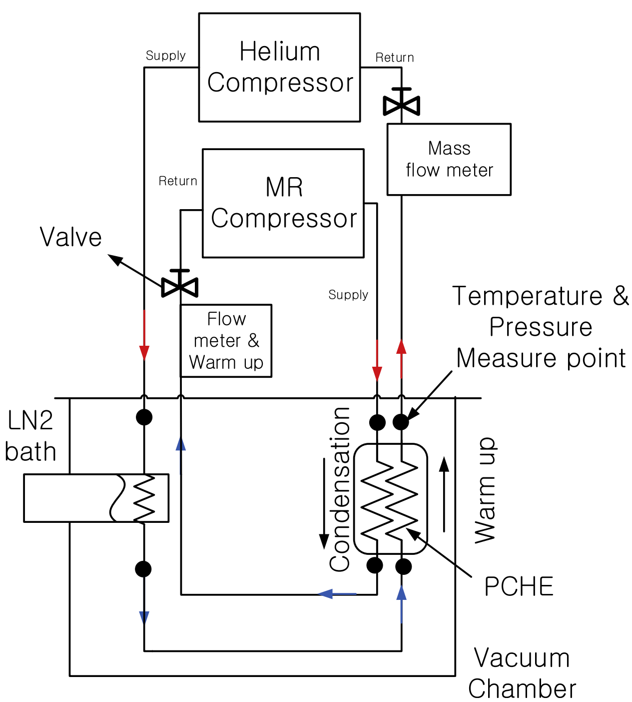


**Fig. 2.** Experimental setup for mixed refrigerant condensation. Mixed refrigerant enters PCHE at 300 K and exit at low temperature approximately 140 K after heat exchanged with cooled helium.

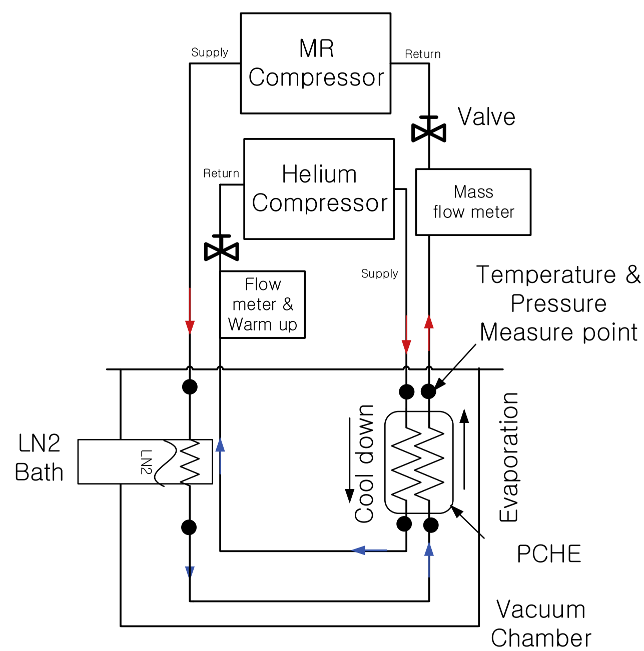


**Fig. 3.** Experimental setup for mixed refrigerant evaporation. Mixed refrigerant enters the PCHE at 130 K and exits at the high temperature of approximately 290 K after heat exchanged with hot helium.

## 2. Experimental setup

### 2.1. Flow circulation loops

Figs. 2 and 3 show schematic diagrams of the experimental setup, composed of two closed fluid loops. The setup has two compressors, the microchannel heat exchanger, the pre-cooler, and the $LN_2$ bath. One helium compressor is employed to generate helium flow, and another helium compressor generates mixed refrigerant flow. The mass flow rate of the mixed refrigerant is measured by a Coriolis flow meter. The helium mass flow rate is measured by another mass flow meter. Four silicon diode thermometers are attached to the surface of the inlet and outlet tubes of the heat exchanger in order to measure the flow temperatures with respect to the mass flow rates. Four pressure transducers are attached to the inlets and outlets of the heat exchanger. Experiments are conducted inside a vacuum chamber in order to eliminate heat ingress from convection during the course of the cryogenic experiment. All the pipes inside the vacuum chamber are soldered to eliminate any leakage of fluids at cryogenic temperatures.

Temperature data are collected by a monitoring device. Mass flow rate and pressures are collected by a data acquisition system. All collected data are recorded by software on a personal computer.

The location of helium and mixed refrigerant compressors are switched with each other to cause evaporation or condensation of the mixed refrigerant. Fig. 2 depicts the flow scheme for condensation of the mixed refrigerant. The mixed refrigerant enters the heat exchanger at 300 K from the mixed refrigerant compressor. At the opposite side, the helium is cooled from the $LN_2$ bath to 120 K, and then enters the test heat exchanger. The mixed refrigerant is condensed by the cold helium. The condensed mixed refrigerant heats again as it exits the vacuum chamber, and proceeds back to the compressor. In Fig. 3, the mixed refrigerant is supplied at 300 K and cooled at the $LN_2$ bath to about 120 K. The mixed refrigerant is heated by the warm helium and fed back to the compressor at a temperature of 290 K. Cold helium enters a water heat exchanger to warm up and return back to the compressor.

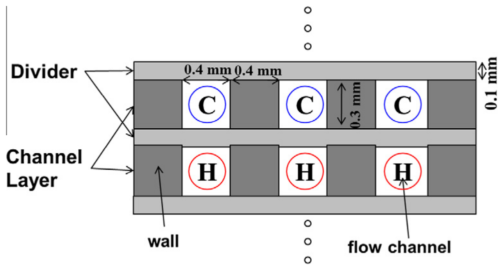


**Fig. 4.** Schematic of construction structure of 20 layer PCHE and dimensions.

### 2.2. Microchannel heat exchanger

The microchannel heat exchanger is composed of thin stainless steel plates stacked together. There are two types of plates, the divider and the channel layers. Fig. 4 shows the schematic cross section area of the heat exchanger. The divider plates are 100 μm and serve as flow separators. The channel layers are configured to form 23 parallel flow channels each with a rectangular cross section made by fully etching the plates. The channel size is 300 μm high and 400 μm wide, as depicted in Fig. 4. Channel flow pathways are composed of several straight sections and 90° curve sections forming a U-shaped path. Half-etching technology, which excavates a half depth of the plate thickness, is applied specifically to only the curved channels to improve mechanical integrity. Otherwise the curved channel walls cannot align with the flow path. The location of the half-etched curvature section is shown in Fig. 5.

Fig. 6 shows the completed PCHE. After alternately stacking the dividers and the channel layers, diffusion bonding is carefully performed in a vacuum furnace to complete the heat exchanger fabrication. An EDM (electrical discharge machining process) is applied to the fabricated PCHE to reduce axial conduction heat transfer. The PCHE is identically composed of 10 hot streams and 10 cold streams in a counter flow arrangement. The PCHE has core dimensions of 220 × 77 × 8 mm$^3$ (20 layers). The 6.35 mm (1/4 in.) diameter stainless steel tubes are welded at each of the four flow sections as headers of the PCHE. The specifications for the fabricated 20-layer PCHE are summarized in Table 2. Because the temperature span of the experiment is large (300–130 K), the axial conduction heat transfer through the heat exchanger body may affect the measurement during the experiment. However, the wire cut PCHE have negligible axial conduction effect [9].

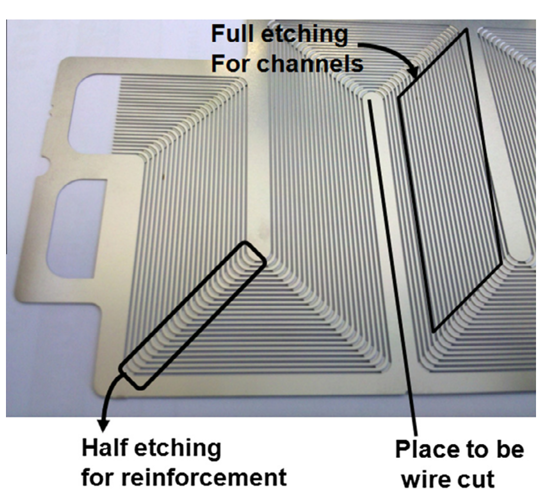


**Fig. 5.** Etched stainless steel plate for the channel layer.

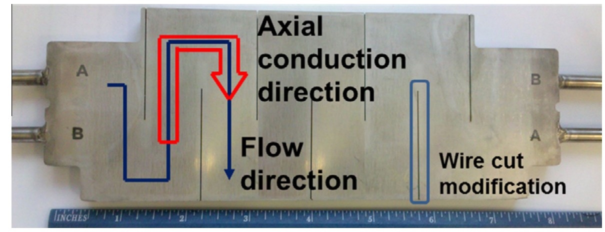


**Fig. 6.** Picture of the microchannel heat exchanger.

**Table 1**
The boiling point and molecular mass of selected refrigerants.

| Refrigerant | Boiling point (K) | Molecular mass (g/mol) |
|---|---|---|
| Argon (Ar) | 87.3 | 39.948 |
| R14 ($CF_4$) | 145.3 | 88.00 |
| R23 ($CHF_3$) | 191.1 | 70.01 |
| R218 ($C_3F_8$) | 236.4 | 188.02 |
| R134a ($CH_2FCF_3$) | 246.8 | 102.03 |

**Table 2**
Specifications of the PCHE used in the experiments.

| Specifications | PCHE |
|---|---|
| Hydraulic diameter | 0.340 mm |
| Heat transfer area | 0.2024 m$^2$ |
| Flow area | 2.64e−5 m$^2$ |
| Length | 0.55 m |
| Volume | 0.136 L |
| Area density | 1490 m$^2$/m$^3$ |

### 2.3. Mixed refrigerant composition

Mixed refrigerants are selected with two constraints. Firstly, non-flammable gases are selected for safety reasons. Secondly, gases are selected with zero ODP (Ozone depletion Potential) values for environmental reason and favorable acceptance as refrigerant. Finally, Argon, R14, R23, R218, and R134a are selected. Each of the pure refrigerants are charged into the closed loop. The mixture composition in terms of mole fractions is of 29% argon, 22% R14, 8% R23, 10% R218, and 31% R134a. The composition of the mixed refrigerant is confirmed with Gas Chromatography. Two standard mixed gas samples are used for the calibration. Table 1 summarizes the boiling point and the molecular weight of the selected refrigerants. Fig. 7 shows the temperature entropy diagram of the selected mixed refrigerant.

## 3. Data reduction

The following equations have been employed to calculate the heat transfer coefficients of the mixed refrigerant from the collected data during each particular test at equilibrium conditions [10]. The heat transfer rate in the evaporation or condensation process can be determined from the heat balance of the helium flow:

$$\dot{Q}_{He} = \dot{m}_{He} c_{p,He} (T_{He,in} - T_{He,out}) \tag{1}$$

The enthalpy values were calculated by REFPROP [11] from the pressure and temperature measured at the inlet and the outlet of the heat exchanger. The heat transfer rate of the mixed refrigerant is calculated with the following equation

$$\dot{Q}_{MR} = \dot{m}_{MR} (i_{in,MR} - i_{out,MR}) \tag{2}$$

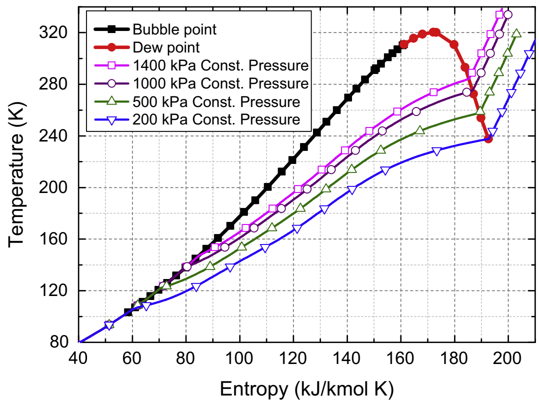


**Fig. 7.** Temperature entropy ($T$–$s$) diagram of mixed refrigerant (Ar:R14:R23:R218:R134a = 29:21:7:9:31 mol%).

The overall heat transfer coefficient based on the heat transfer area of the test section is:

$$U = \frac{\dot{Q}}{A_{HT}\Delta T_{LMTD}}, \tag{3}$$

where $\Delta T_{LMTD}$ is the logarithmic mean temperature difference based on the inlet and outlet temperatures of the helium/mixed refrigerant flows. The average value of helium heat transfer rate and mixed refrigerant heat transfer rate is used for $\dot{Q}$. Assuming no fouling, and very small thermal resistance of the heat exchanger wall, the heat transfer coefficient of the mixed refrigerant ($h_{MR}$) can be calculated as follows:

$$\frac{1}{h_{MR}} = \frac{1}{U} - \frac{1}{h_{He}} \tag{4}$$

Axial conduction of the heat exchanger is neglected as previously described. The heat transfer coefficient of the helium is analyzed in the previous research [12]. The heat transfer coefficients were validated with the preliminary experiments. The equations from Peng and Peterson [13] are used to obtain the heat transfer coefficient and friction factor of single phase flow of helium.

The amount of heat transfer between two fluids, calculated by Eqs. (1) and (2), is measured and compared in Fig. 8. The heat balance error between helium and mixed refrigerant is less than 10%. The uncertainty of the measured data is determined with the following equation,

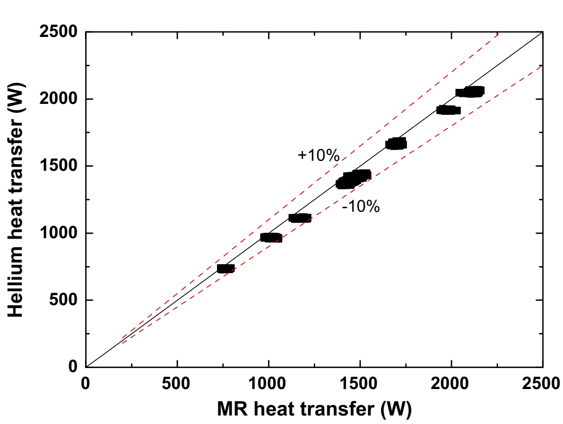


**Fig. 8.** The heat balance between mixed refrigerant and helium in the microchannel heat exchanger.

**Table 3**
Uncertainty analysis.

| Measurement | Number | Error |
|---|---|---|
| Temperature | 4 | ±0.1 K (surface mount) |
| Pressure | 4 | ±0.5% |
| Mass flow rate | 2 | ±0.5% |
| Gas chromatography | 1 | ±1.0% |
| REFPROP calculation | 1 | ±0.001% |
| Total uncertainty | | ~5% |

$$U = \sqrt{B^2 + \left(t_{95\%,\nu}\frac{S}{\sqrt{N}}\right)^2} \tag{5}$$

where $B$ is the total bias error and $S$ is the standard deviation of the data. Table 3 shows the error of the measurement and the total uncertainty. The experimental results show an uncertainty of around 5%.

## 4. Experimental results

### 4.1. Two phase heat transfer coefficients

The experiment is performed to first observe the condensation heat transfer characteristic of the mixed refrigerant. Fig. 9(a) shows the temperature of the inlets and outlets of the heat exchanger with time. Helium is cooled with a $LN_2$ bath and the temperature is maintained approximately at 130 K. The room temperature (300 K) gas-phase mixed refrigerant enters the heat exchanger and is condensed by the cold helium. The outlet temperature of the mixed refrigerant becomes around 150 K. The pressure of the mixed refrigerant during the condensation experiment is maintained around 800 kPa. The quality at the outlet of the heat exchanger is calculated to be 0.22. Fig. 9(b) displays the mass flow rate of the mixed refrigerant and helium. The mass flow rate of the mixed refrigerant is increased to observe its effect on the heat transfer coefficient. The helium mass flow rate is increased to maintain the heat balance between the two fluids and to maintain the inlet/outlet temperature of the mixed refrigerant and helium. Due to the constant inlet and outlet temperature of helium and mixed refrigerant, the heat flux to each fluid is increased as the mass flow rate is increased.

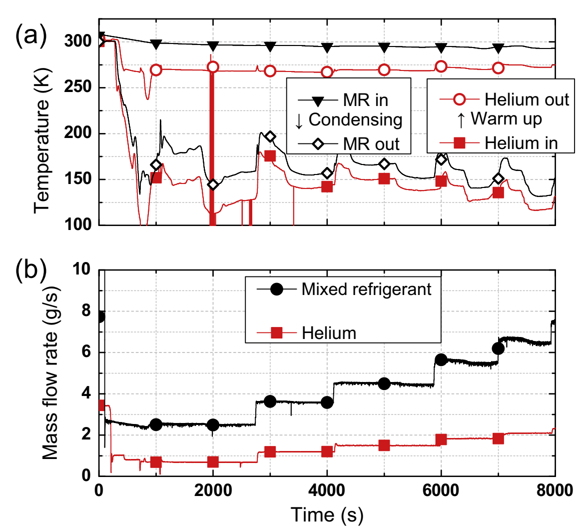


**Fig. 9.** Experimental results on mixed refrigerant condensation process. (a) Temperature at heat exchanger outlets with time and (b) mass flow rate of mixed refrigerant and helium with time.

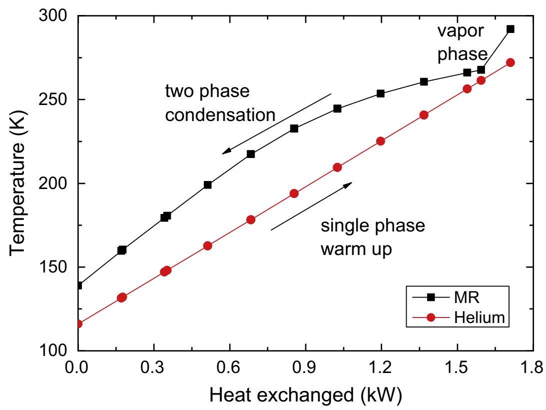


**Fig. 10.** Calculated temperature profile in the heat exchanger. Helium is cold fluid (2.1 g/s) and mixed refrigerant (6.5 g/s) is hot fluid in the heat exchanger.

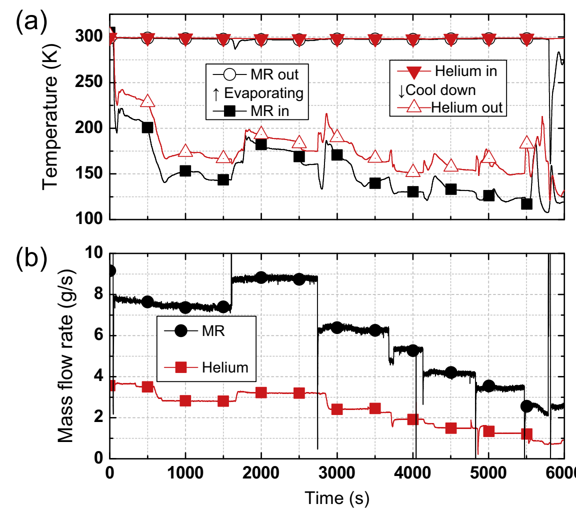


**Fig. 12.** Experimental results on evaporation process of mixed refrigerant. (a) Temperature at heat exchanger outlets with time and (b) mass flow rate of mixed refrigerant and helium with time.

Fig. 10 shows the calculated temperature profile in the heat exchanger during the mixed refrigerant condensation experiment. The profile is calculated by Aspen HYSYS [14] using the Peng–Robinson equation of state. The mass flow rates of the mixed refrigerant and helium are 6.5 g/s and 2.1 g/s, respectively. The temperature profile of the mixed refrigerant exhibits a rapid decrease at the high temperature range, because it is cooled down to the vapor phase. After entering the two-phase range, the temperature decreases slowly due to the contribution of latent heat.

Fig. 11 presents the variation in the heat transfer coefficients of the mixed refrigerant with increasing mass flow rate from 0 to 7 g/s (250 kg/m$^2$ s in mass flux) and heat flux (10–15 kW/m$^2$). The overall heat transfer coefficient is calculated by Eq. (3) from the measurements of temperature, pressure, and mass flow rate. Also, single phase heat transfer coefficient of helium is plotted for comparison [13]. The condensation heat transfer coefficient of the mixed refrigerant is calculated by Eq. (4). The calculated heat transfer coefficients show lower values than 1000 W/m$^2$ K for the given mass flow rates. Linear fit to the data is performed on the experimental condensation heat transfer coefficient values for the mixed refrigerant and it is also plotted as the red line in Fig. 11.

The experiment was continued to investigate the evaporative heat transfer characteristics of the mixed refrigerant. Fig. 12(a) shows the typical experimental results of the inlet/outlet temperatures of the heat exchanger. The mixed refrigerant is cooled at the $LN_2$ bath to approximately 130 K and enters the heat exchanger. Helium at 300 K enters the heat exchanger and is cooled by the cold mixed refrigerant. The outlet temperature of the helium is close to 160 K. Fig. 12(b) displays the mass flow rate of the mixed refrigerant and helium. The mass flow rate of the mixed refrigerant is changed intentionally to observe its effect on the heat transfer coefficient. The helium mass flow rate is also changed to maintain the inlet/outlet temperatures of the two fluids. The pressure of the mixed refrigerant is maintained between 400 kPa and 600 kPa.

Fig. 13 shows the calculated temperature profile in the heat exchanger during the evaporation experiment with the mixed refrigerant. This condition represents mass flow rates for the mixed refrigerant and helium of 4.3 g/s and 1.5 g/s respectively. The temperature profile of the mixed refrigerant exhibits a slow increase at the low temperature range, because it is in the two-phase regime. After entering the single phase region during the warm-up process, the temperature increases sharply. Fig. 14 presents the variation in the heat transfer coefficients for the fluids for increasing mass flow rates from 0 to 9 g/s. The evaporation heat transfer coefficient of the mixed refrigerant shows an increasing tendency commensurate with the increase in mass flow rate. The evaporation heat transfer coefficients vary from 1000 W/m$^2$ K to 5000 W/m$^2$ K for

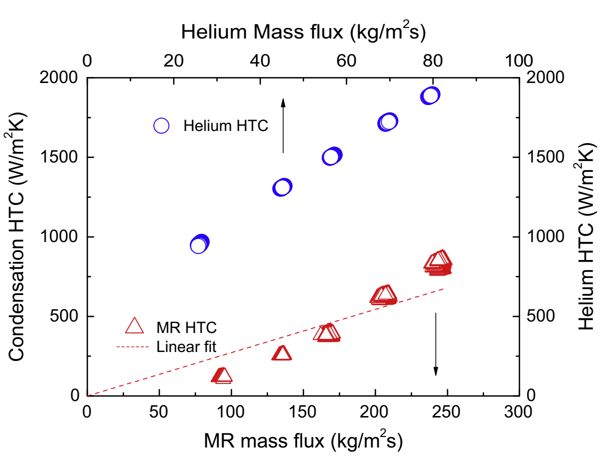


**Fig. 11.** Condensation heat transfer coefficient of mixed refrigerant (red), and single phase heat transfer coefficient of helium (blue) with mass flow rate. Linear interpolation performed on heat transfer coefficient values of the mixed refrigerant. (For interpretation of the references to color in this figure legend, the reader is referred to the web version of this article.)

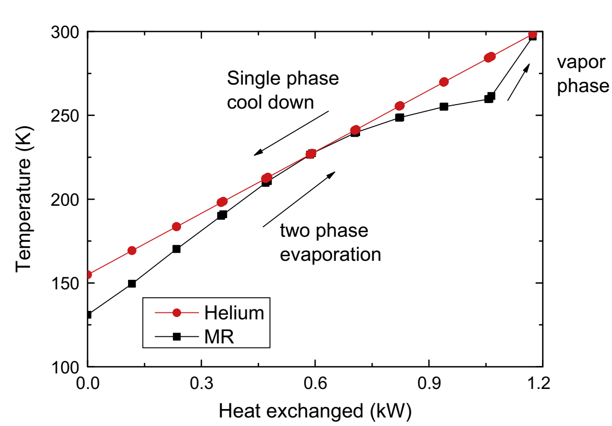


**Fig. 13.** Temperature profile in the heat exchanger. Helium is cold fluid and mixed refrigerant is hot fluid in the heat exchanger.

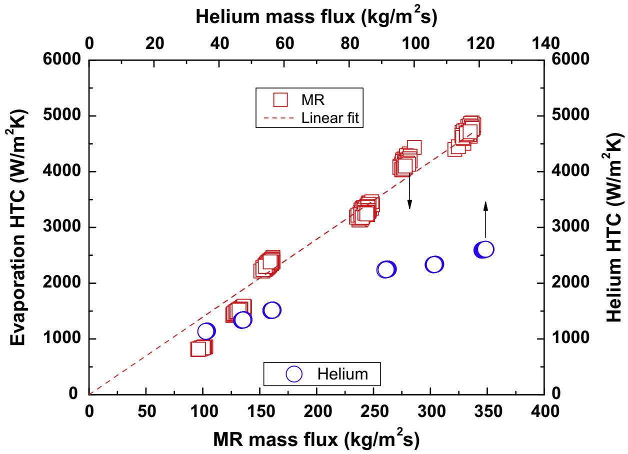


**Fig. 14.** Evaporation heat transfer coefficient of mixed refrigerant (red), and single phase heat transfer coefficient of helium (blue) with mass flow rate. Linear interpolation performed to calculated heat transfer coefficient of mixed refrigerant. (For interpretation of the references to color in this figure legend, the reader is referred to the web version of this article.)

the given mass flux. The linear fit to the data is performed and plotted as dash line in Fig. 14.

### 4.2. Validation experiment

Another experiment has been conducted to confirm the experimental two-phase heat transfer coefficient values of the mixed refrigerant. Fig. 15 shows the experimental setup for the validation. The closed loop of the mixed refrigerant is comprised of the compressor, the microchannel heat exchanger used in the previous experiment, and the $LN_2$ bath. In this setup, the mixed refrigerant is circulated by the compressor and passes through the heat exchanger. The mixed refrigerant from the heat exchanger is thermally conditioned by the $LN_2$ bath to yield a constant temperature of approximately 130 K, and then returns to the heat exchanger, where its temperature increases to almost 300 K after passing through it. This setup is similar to the Joule–Thomson refrigerator operation except that the Joule–Thomson valve is substituted by the $LN_2$ bath to generate a constant cold temperature. Therefore, condensation takes place in the high pressure (or hot) side and evaporation takes place in the low pressure (or cold) side of the heat exchanger.

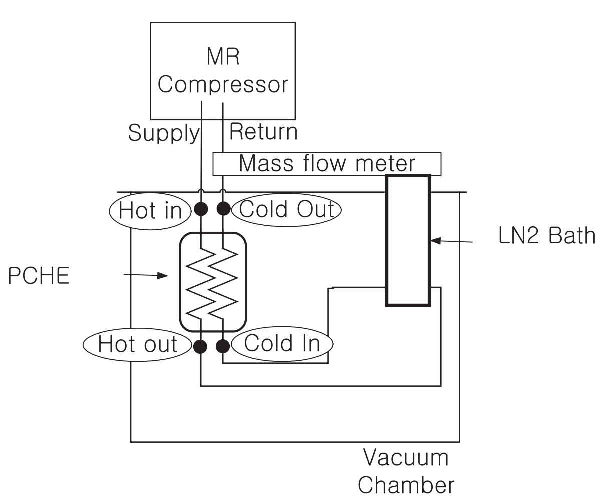


**Fig. 15.** Experimental setup for validation of measured heat transfer coefficients.

In this experimental setup, the overall heat transfer coefficients for different mass flux can be obtained, whereas the overall heat transfer coefficient is expressed with the local heat transfer coefficients as Eq. (6)

$$\frac{1}{U} = \frac{1}{h_{cond}} + \frac{1}{h_{evap}} \tag{6}$$

Fig. 16 shows the experimental values of the overall heat transfer coefficient calculated by Eq. (3) for increasing mass flux. The linearly fitted heat transfer coefficients for condensation and evaporation from Figs. 11 and 14 are used to calculate the overall heat transfer coefficient using Eq. (6). The calculated overall heat transfer coefficients are displayed as a line to be compared with the experimental values in Fig. 16. The calculated values and the experimental values show similar increasing tendency with respect to each other, which means that there is negligible heat transfer resistance. Moreover, this experiment demonstrates that the two-phase heat transfer coefficients, those determined separately from the mixed refrigerant-helium experiments, are correct, because the overall heat transfer coefficients are a function of the local heat transfer coefficients.

## 5. Comparison with correlations

After the validation of the local heat transfer coefficients, the experimental heat transfer coefficient values are compared with previous heat transfer coefficient correlations. For condensation heat transfer coefficients, research has been conducted by Bandhauer [15] with R134a in microchannel tubes ($D_h \sim 700$ μm). This research compared numerous heat transfer coefficient correlations to experimental values. Radermacher and Hwang [8] summarized the heat transfer coefficient correlations for mixed refrigerants. However, the mixed refrigerant used in this reference were composed of room temperature refrigerants such as R134a, R407c, and R22. The typical hydraulic diameter employed to measure the heat transfer coefficient was larger than 7 mm.

In this section, the heat transfer coefficient is calculated with the conventional correlations and compared to the experimental values from the previous section. Since the flow pattern of the mixed refrigerant in the microchannel is assumed to have annular characteristics [16], the correlations for annular flow were examined. The equations developed by Soliman [17], Cavallini and Zecchin [18], Moser et al. [19], Chen [20], Travis [21], Dobson and Chato [22], and Shah [23] are compared to the experimental data. Lastly, the general heat transfer coefficient correlation developed by Dittus and Boelter [24] is compared. These equations calculate

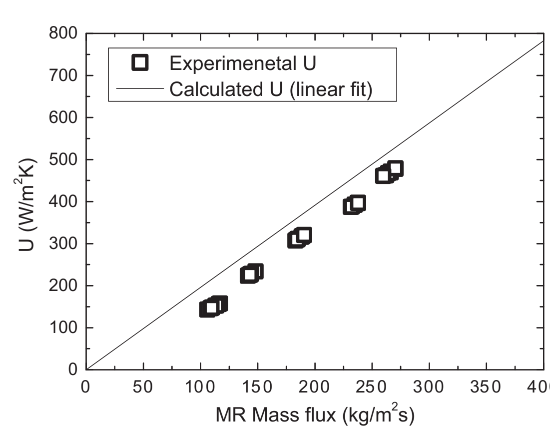


**Fig. 16.** The experimental overall heat transfer coefficient compared with the linear fitted experimental results.

**Table 4**
The condensation heat transfer coefficient correlations.

| Author(s) | Correlations |
|---|---|
| Soliman [17] | $h = 0.036\frac{k_l\rho_l^{0.5}}{\mu_l}\mathrm{Pr}_l^{0.65}(\tau_m+\tau_f)^{0.5}$<br>$\tau_m = \frac{D_h}{4}\left(\frac{G^2}{\rho_v}\right)\frac{\Delta x}{\Delta z}\sum_{n=1}^{5}a_n\left(\frac{\rho_v}{\rho_l}\right)^{n/3}, Re_{vo} = \frac{GD_h}{\mu_v}$<br>$\tau_f = 0.0225\frac{G^2}{\rho_v}Re_{vo}^{-0.2}\left(x^{1.8}+5.7\left(\frac{\mu_l}{\mu v}\right)^{0.0523}(1-x)^{0.47}x^{1.33}\left(\frac{\rho_v}{\rho_l}\right)^{0.261}+8.11\left(\frac{\mu_l}{\mu_v}\right)^{0.105}(1-x)^{0.94}x^{0.86}\left(\frac{\rho_v}{\rho_l}\right)^{0.522}\right)$ |
| Cavallini and Zecchin [18] | $Nu = 0.0344Re_{lo}^{0.83}\left(1+x\left[\left(\frac{\rho_l}{\rho_v}\right)^{0.5}-1\right]\right)^{0.82}\mathrm{Pr}_l^{0.35}, Re_{lo} = \frac{GD_h}{\mu_l}$ |
| Moser [19] | $Nu = \frac{0.0994^{0.126\mathrm{Pr}_l^{-0.448}}Re_l^{-0.113\mathrm{Pr}_l^{-0.563}}Re_{eq}^{1+0.11025\mathrm{Pr}_l^{-0.448}}\mathrm{Pr}_l^{0.815}}{(1.58\ln Re_{eq}-3.28)(2.58\ln \mathrm{Re}_{eq}+13.7\mathrm{Pr}_l^{2/3}-19.1)}$<br>$Re_{eq} = \phi_{lo}^{8/7}Re_{lo}, \phi_{lo}^2 = E+\frac{3.24H}{Fr_{tp}^{0.045}We_{tp}^{0.035}}$ |
| Chen [20] | $Nu = 0.036\mathrm{Pr}_l^{0.65}(Re_{lo}-Re_l)^{0.7}Re_l^{0.2}\sqrt{\left(\frac{0.252\mu_l^{1.177}\mu_v^{0.156}}{D_h^2g^{2/3}\rho_l^{0.553}\rho_v^{0.78}}\right)}$<br>$Re_{lo} = \frac{GD_h}{\mu_l}, Re_l = \frac{G(1-x)D_h}{\mu_l}, Nu = \frac{h}{k_l}\left(\frac{\mu_l^2}{\rho_l^2g}\right)^{1/3}$ |
| Traviss [21] | $h = \frac{k_l}{D}F(X_{tt})\frac{Re_l^{0.9}\mathrm{Pr}_l}{F_2}$<br>$F(X_{tt}) = 0.15\lvert X_{tt}^{-1}+2.85X_{tt}^{-0.476}\rvert, F_2 = f(Pr_l, Re_l)$ |
| Dobson [22] | $h = \frac{k_l}{D}0.023Re_l^{0.8}\mathrm{Pr}_l^{0.4}(1+2.22X_{tt}^{-0.89})$for annular flow regime |
| Shah [23] | $h = h_l\left((1-x)^{0.8}+\frac{3.8x^{0.76}(1-x)^{0.04}}{p_r^{0.38}}\right)$<br>$h_l =$ single phase liquid heat transfer coefficient – Dittus Boelter |
| Dittus Boelter [24] | $Nu = 0.023Re_{tp}^{0.8}\mathrm{Pr}_l^{0.4}$<br>$Re_{tp} = \frac{GD_h}{\bar{\mu}}$ |

the heat transfer coefficients as a function of quality (or temperature), mass flux, hydraulic diameter, and fluid properties. The heat flux is neglected in the selected correlations.

Table 4 summarizes the condensation heat transfer coefficient correlation used in this paper. MATLAB and REFPROP [11] are utilized to calculate the condensation heat transfer coefficient as a function of the temperature and quality. The Peng–Robinson equation of state is used for the calculation.

The condensation heat transfer coefficients are calculated as a function of quality. Due to the unique characteristics of a mixed refrigerant, the quality varies with the temperature. Therefore, the heat transfer coefficient can be calculated as function of the temperature. Fig. 17 displays the condensation heat transfer coefficient of the given mixed refrigerant at various values of temperatures and at given mass flux and pressure. The predicted heat transfer coefficients from Travis, Shah, Dobson, Cavallini show high values at high quality (or high temperature), and show low values at low quality (or low temperature). The heat transfer coefficient values predicted by Moser, Soliman, and Chen show comparably lower values. The Dittues–Boelter equation using average fluid properties calculates heat transfer coefficient values similar to those of single phases.

These predicted heat transfer coefficients are averaged along the length with the Eq. (7) to compare with the experimental results.

$$\bar{h}_L = \frac{1}{L}\int_0^L h_z dz \tag{7}$$

Fig. 18 displays the predicted average heat transfer coefficients over the heat exchanger length and the experimentally obtained heat transfer coefficients with different mass flux. The average absolute deviations (AAD) are calculated for the predicted results in order to understand the applicability of the correlations. The AAD is calculated through the following equation

$$AAD = \frac{1}{N}\sum\frac{|h_{exp}-h_{pred}|}{h_{exp}} \tag{8}$$

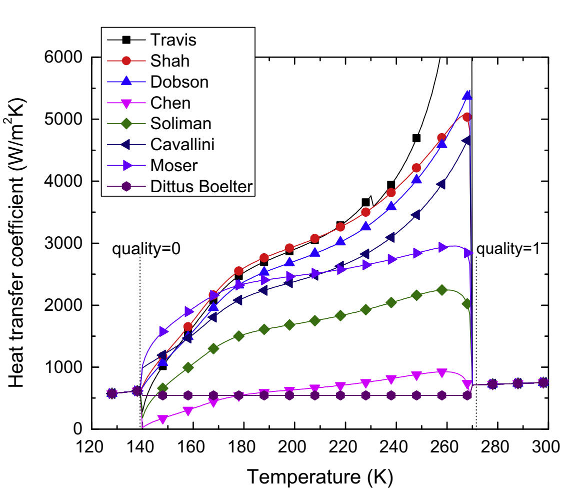


**Fig. 17.** Predicted condensation heat transfer coefficients with temperature at $G = 200$ kg/m$^2$ s, $P = 800$ kPa.

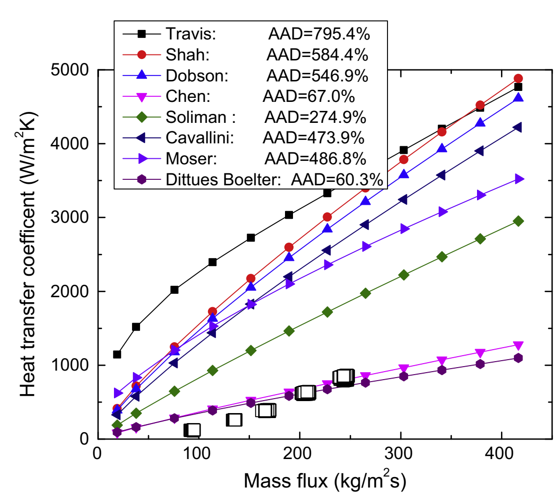


**Fig. 18.** Comparison of condensation heat transfer coefficients with predicted and experimental data.

The AAD for all the correlations calculated is displayed in Fig. 18. It is clear that the prediction method from Chen [20] and Dittus Boelter predict condensation heat transfer coefficient of mixed refrigerant in the range of 60–70% of AAD. The obtained experimental heat transfer coefficient values show somewhat lower values than the previous experimental results [25] for single component two-phase fluid. Note that the correlations from Travis, Shah, Dobson and Cavallini are developed for pure fluids. It is known that the local condensation heat transfer coefficients of the mixtures are smaller than those of pure refrigerants. The degradation of heat transfer coefficient varies up to 50% that of the pure refrigerants [8]. The apparently low heat transfer coefficient for a cryogenic mixed refrigerant may be induced from the large mass transfer resistance during the phase change process. Due to the lack of experimental data of heat transfer coefficient for cryogenic mixed refrigerants, it is difficult to compare with the references. More precise experiments for condensation of mixed refrigerants to measure heat transfer coefficients is required to validate the current experimental data.

The evaporation heat transfer coefficients of mixed refrigerants are calculated with different correlations. Table 5 summarizes the various correlations used for the calculations. A considerable number of heat transfer correlations of flow boiling for pure fluids have been proposed. Chen [26], Bennett–Chen [27], and Gungor–Winterton [28] developed correlations based on the superposition model, which divides the heat transfer into two parts: a nucleate pool boiling contribution ($h_{nb}$) and a bulk convective contribution ($h_{bc}$). Later, Gungor–Winterton [29] modified their correlation into an enhancement model, which enhances the single-phase heat transfer coefficient of the flowing liquid by a two-phase enhancement factor. Liu–Winterton [30], and Wattelet [31] proposed correlations based on the asymptotic models.

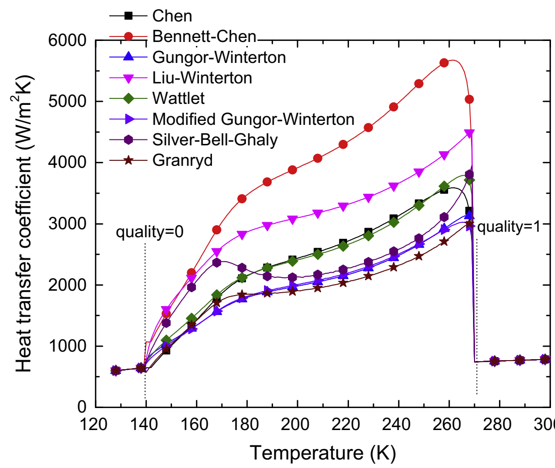


**Fig. 19.** Predicted evaporation heat transfer coefficients with temperature, $G = 200\ \mathrm{kg/m^2\ s}$, $P = 800$ kPa.

Little [32] developed a heat transfer coefficient correlation based on the annular flow regime. Moreover, Ardhapurkar [33] compared the correlations developed by Silver–Bell–Ghaly [34,35] and Granryd [36]. Little and Ardhapurkar compared their correlations to experimental data obtained from Nellis [5]. Nellis measured the evaporative heat transfer coefficient of nitrogen–methane–ethane–propane–butane at different mass flux and pressure. Ardhapurkar indicated that the Silver–Bell–Ghaly and Granryd correlations can be used to predict local evaporative heat transfer coefficient of nitrogen–hydrocarbon cryogenic mixed refrigerants.

**Table 5**
The evaporation heat transfer coefficient correlations.

| Authors | Correlations |
|---|---|
| Chen [26] | $h = h_{nb} + h_{bc}$<br>$h_{bc} = 0.023\frac{k_l}{D}Re_{tp}^{0.8}\mathrm{Pr}_l^{0.4}, Re_{\mathrm{tp}} = \frac{G(1-x)D}{\mu_l}F(X_{tt})^{1.25}$<br>$h_{nb} = 0.00122\left(\frac{k_l^{0.79}c_{p,l}^{0.45}\rho_l^{0.49}}{\sigma^{0.5}\mu_l^{0.29}i_{fg}^{0.24}\rho_{fg}^{0.24}}\right)[T_w - T_{sat}(P_l)]^{0.24}[P_{sat}(T_w) - P_l]^{0.75}S$ |
| Bennett–Chen [27] | $h = h_{nb} + h_{bc}$<br>$h_{bc} = h_lF(X_{tt})Pr_l^{0.296}, h_l = 0.023\frac{k_l}{D}Re_l^{0.8}\mathrm{Pr}_l^{0.4}$<br>$h_{nb} = 0.00122\left(\frac{k_l^{0.79}c_{pl}^{0.45}\rho_l^{0.49}}{\sigma^{0.5}\mu_l^{0.29}h_{fg}^{0.24}\rho_{fg}^{0.24}}\right)[T_w - T_{sat}(P_l)]^{0.24}[P_{sat}(T_w) - P_l]^{0.75}S$ |
| Gungor–Winterton [28] | $h = Eh_l + Sh_{pool}$<br>$h_l = 0.023\left(\frac{k_l}{D_h}\right)\left[(1-x)\frac{GD_h}{\mu}\right]^{0.8}\mathrm{Pr}_l^{0.4}, h_{pool} = 55P_r^{0.12}(-\log_{10}P_r)^{-0.55}M^{-0.5}q^{0.67}$<br>$E = 1 + 24000Bo^{1.16} + 1.37X_{tt}^{-0.86}, S = \left(1 + 1.15\times10^{-6}E^2Re_l^{1.17}\right)^{-1}$ |
| Modified Gungor–Winterton [29] | $h_{tp} = E_{new}h_{lo}$<br>$h_{lo} = 0.023\left(\frac{k_l}{D}\right)\left[(1-x)\frac{GD}{\mu}\right]^{0.8}\mathrm{Pr}_l^{0.4}$<br>$E_{new} = 1 + 3000(Bo\cdot F_c)^{0.86} + 1.12(\frac{x}{1-x})^{0.75}\left(\frac{\rho_l}{\rho_v}\right)^{0.41}$ |
| Liu–Winterton [30] | $h = \sqrt{(Eh_l)^2 + (Sh_{pool})^2}$<br>$E = [1 + x\mathrm{Pr}_l\left(\frac{\rho_l}{\rho_v} - 1\right)]^{0.35}$<br>$S = (1 + 0.055E^{0.1}Re_l^{0.16})^{-1}$ |
| Wattelet [31] | $h = [h_{nb}^{2.5} + h_{bc}^{2.5}]^{1/2.5}$<br>$h_{nb} = 55M^{-0.5}q^{0.67}P_r^{0.12}[-\log_{10}P_r]^{-0.55}$<br>$h_{bc} = Fh_lR$ |
| Silver–Bell–Ghaly [34,35] | $\frac{1}{h_m} = \frac{1}{h_c} + \frac{Z_g}{h_v}$<br>$h_c = E_{new}h_{lo}, Z_g = x\cdot Cp_v\cdot\frac{dT_{dew}}{di}$<br>$E_{new} = 1 + 3000(Bo\cdot F_c)^{0.86} + 1.12(\frac{x}{1-x})^{0.85}\left(\frac{\rho_l}{\rho_v}\right)^{0.7}$ |
| Granryd [36] | $\frac{h_m}{h_{lo}} = \frac{F_p}{(1+A)} = F_m$<br>$F_p = 2.37\left(0.29 + \frac{1}{X_{tt}}\right)^{0.85}$<br>$A = \left(\frac{F_p}{C_{\mathrm{lg}}}\right)x^2\left[\left(\frac{1-x}{x}\right)\left(\frac{\mu_v}{\mu_l}\right)\right]^{0.8}\left(\frac{\mathrm{Pr}_l}{\mathrm{Pr}_v}\right)^{0.4}\left(\frac{k_l}{k_v}\right)\left(\frac{Cp_v}{Cp_w}\right), Cp_w = \left(\frac{\partial i}{\partial T}\right)_P$ |

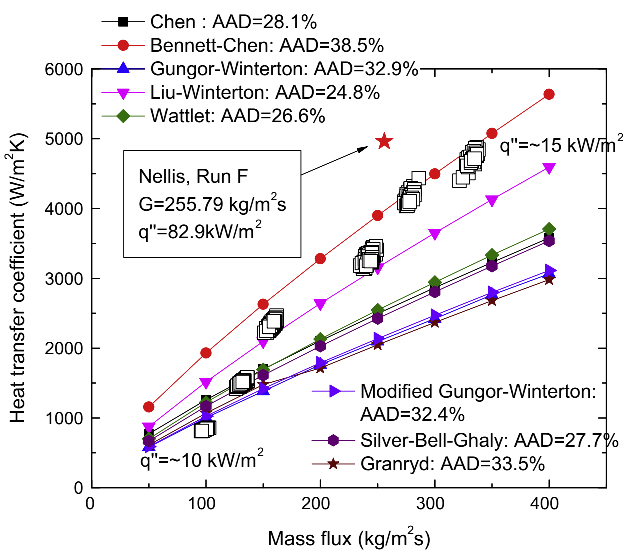


**Fig. 20.** Comparison of evaporation heat transfer coefficients with predicted and experimental data.

The correlations given in Table 5 are calculated and compared to the current experimental results. The correlations shown in Table 5 are mostly developed for the macrochannels, however, several papers [37–39] indicate that these equations show comparable heat transfer coefficient value with those of experiments at small and microchannels. During the calculations, the wall temperature is required to calculate the heat transfer coefficient. The average temperature of helium and mixed refrigerant is assumed to be the wall temperature.

Fig. 19 displays the predicted heat transfer coefficients at different temperature and quality. The heat transfer coefficient values exhibit a wave shape with increasing temperature, where values increase sharply at low quality and high quality regions which is observed from the experimental data of Nellis [5]. Fig. 20 displays the average heat transfer coefficient for varying mass flux. The experimental data are also shown in this plot. The AAD is also obtained and displayed in Fig. 20. The correlations developed by Liu and Winterton, Wattelet, Silver–Bell–Ghaly predict well the experimental evaporation heat transfer coefficients.

The average evaporation heat transfer coefficient for a nitrogen-hydrocarbon mixed refrigerant is also displayed in Fig. 19. The Run-F from Nellis [5] has comparable mass flux of 255.79 kg/m$^2$ s. The heat flux to the channel is larger than the current experiment, however, the heat transfer coefficient value shows similar order of magnitude with the current experimental data.

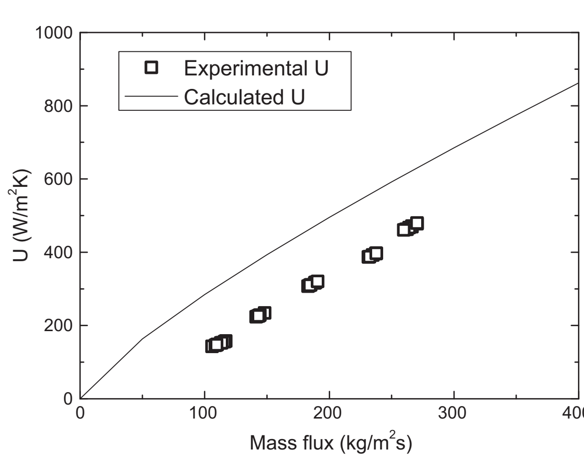


**Fig. 21.** Comparison results of overall heat transfer coefficients: calculated value with Liu-Winterton and Dittus Boelter correlations and experimental data.

The correlations that predict well the heat transfer coefficients are evaluated again in terms of overall heat transfer coefficients. The Dittus–Boelter equation and Liu–Winterton equations are used to calculate the overall heat transfer coefficients ($U$) with Eq. (6). Fig. 21 shows the comparison of the overall heat transfer coefficients between the prediction and experimental data. The predicted overall coefficients show higher values than the experimental values, however the trend is very similar to the experimental data.

## 6. Conclusions

Two-phase heat transfer coefficients of the argon–freon mixed refrigerant are measured and estimated by the LMTD heat exchanger analysis. The condensation heat transfer coefficient shows low values below 1000 W/m$^2$ K for the given mass flux of 0–250 kg/m$^2$ s. However, the evaporation heat transfer coefficient shows high values around 5000 W/m$^2$ K at 350 kg/m$^2$ s. The overall heat transfer coefficients are calculated using the experimentally obtained local heat transfer coefficients, and these values are compared to the experimental overall heat transfer coefficients. This comparison confirms that the local heat transfer coefficients are correct and reasonable. The condensation and evaporation heat transfer coefficients are compared to general two-phase heat transfer coefficient correlations. Chen and Dittus–Boelter correlations serve well for the mixed refrigerant condensation heat transfer coefficient. The experimental evaporation heat transfer coefficient is compared to the correlations developed for pure and mixed refrigerants. The Liu–Winterton correlation show the minimum AAD with respect to the experimental data. These results can be useful when designing microchannel heat exchangers for Joule Thomson refrigerators using argon–freon gases. More experimental data of two-phase cryogenic mixed refrigerants in microchannels are required for better estimation of the heat transfer coefficient that is valuable information for cryogenic heat exchanger design parameters.

## Acknowledgments

This research is supported by a grant from Space Core Technology Development Program of National Research Foundation – South Korea (NRF-2013-042033) funded by Ministry of Science, ICT & Future Planning (MSIP).

## References

[1] Venkatarathnam G. Cryogenic mixed refrigerant processes. Springer; 2008.
[2] Alexeev A, Haberstroh C, Quack H. Study of behavior in the heat exchanger of a mixed gas Joule–Thomson cooler. Adv Cryogenic Eng 1997;2:431667–75.
[3] Gong M, Wu J, Luo E, Qi Y, Hu Q, Zhou Y. Study on the overall heat transfer coefficient for the tube-in-tube heat exchanger used in mixed-gases coolers. In: Advances in cryogenic engineering: transactions of the cryogneic engineering conference; 2002. p. 1483–90.
[4] Ardhapurkar P, Sridharan A, Atrey M. Investigations on two-phase heat exchanger for mixed refrigerant Joule–Thomson cryocooler. Advances in cryogenic engineering: transactions of the cryogenic engineering conference – CEC, vol. 57. AIP Publishing; 2012. p. 706–13.
[5] Nellis G, Hughes C, Pfotenhauer J. Heat transfer coefficient measurements for mixed gas working fluids at cryogenic temperatures. Cryogenics 2005;45(8):546–56.
[6] Cheng L, Mewes D. Review of two-phase flow and flow boiling of mixtures in small and mini channels. Int J Multiph Flow 2006;32(2):183–207.
[7] Celata GP, Cumo M, Setaro T. A review of pool and forced convective boiling of binary mixtures. Exp Thermal Fluid Sci 1994;9(4):367–81.
[8] Radermacher R, Hwang Y. Vapor compression heat pumps with refrigerant mixtures. CRC Press; 2005.

[9] Baek S, Kim J-H, Jeong S, Jung J. Development of highly effective cryogenic printed circuit heat exchanger (PCHE) with low axial conduction. Cryogenics 2012;52(7–9):366–74.

[10] Sami SM, Song B. Heat transfer and pressure drop characteristics of HFC quaternary refrigerant mixtures inside horizontal enhanced surface tubing. Appl Therm Eng 1996;16(6):461–73.

[11] Lemmon EW, Huber ML, McLinden MO. NIST Standard reference database 23: reference fluid thermodynamic and transport properties – REFPROP. Version 9.0 ed: National Institute of Standards and Technology, Standard Reference Data Program, Gaithersburg; 2010.

[12] Baek S, Kim J, Hwang G, Jeong S. Elongating axial conduction path design to enhance performance of cryogeinc compact PCHE (Printed Circuit Heat Exchanger). AIP Conf Proc 2012;1434(1):631–8.

[13] Peng XF, Peterson GP. Convective heat transfer and flow friction for water flow in microchannel structures. Int J Heat Mass Transf 1996;39(12):2599–608.

[14] AspenTech. Aspen HYSYS User Guides. V7.1 ed. Cambridge, MA, USA2008. p. Aspen HYSYS.

[15] Bandhauer TM. Heat transfer in microchannel geometries during condensation of R-134a [MS]. Iowa State University; 2002.

[16] Lewis R, Wang Y, Schneider H, Lee YC, Radebaugh R. Study of mixed refrigerant undergoing pulsating flow in micro coolers with pre-cooling. Cryogenics 2013:57140–9.

[17] Soliman HM. The mist-annular transition during condensation and its influence on the heat transfer mechanism. Int J Multiph Flow 1986;12(2): 277–88.

[18] Cavallini A, Zecchin R. A dimensionless correlation for heat transfer in forced convection condensation. In: Proceedings of the sixth international heat transfer conference; 1974. p. 309–13.

[19] Moser KW, Na B, Webb RL. A new equivalent reynolds number model for condensation in smooth tubes. J Heat Transfer 1998;120(2):410–7.

[20] Chen SL, Gerner FM, Tien CL. General film condensation correlations. Exp Heat Transfer 1987;1(2):93–107.

[21] Traviss DP, Baron AG, Rohsenow WM. Forced-convection condensation inside tubes. Cambridge (Mass.): MIT Heat Transfer Laboratory; 1971.

[22] Dobson M, Chato J. Condensation in smooth horizontal tubes. J Heat Transfer 1998;120(1):193–213.

[23] Shah M. A general correlation for heat transfer during film condensation inside pipes. Int J Heat Mass Transf 1979;22(4):547–56.

[24] Dittus F, Boelter L. Heat transfer in automobile radiators of the tubular type. University of California Publications in Engineering; 1930. p. 2371.

[25] Su Q, Yu GX, Wang HS, Rose JW. Microchannel condensation: correlations and theory. Int J Refrig 2009;32(6):1149–52.

[26] Chen JC. Correlation for boiling heat transfer to saturated fluids in convective flow. Ind Eng Chem Proc Des Develop 1966;5(3):322–9.

[27] Bennett DL, Chen JC. Forced convective boiling in vertical tubes for saturated pure components and binary mixtures. AIChE J 1980;26(3):454–61.

[28] Gungor KE, Winterton RHS. A general correlation for flow boiling in tubes and annuli. Int J Heat Mass Transf 1986;29(3):351–8.

[29] Gungor KE, Winterton RHS. Simplified general correlation for saturated flow boiling and comparisons of correlations with data. Chem Eng Res Des 1987;65(2):148–56.

[30] Liu Z, Winterton RHS. A general correlation for saturated and subcooled flow boiling in tubes and annuli, based on a nucleate pool boiling equation. Int J Heat Mass Transf 1991;34(11):2759–66.

[31] Wattelet JP, Chato JC, Souza AL, Christoffersen BR. Evaporative characteristics of R-12, R-134a, and MP-39 at low mass fluxes. ASHRAE Trans. 1994;100:1603–15.

[32] Little WA. Heat transfer efficiency of kleemenko cycle heat exchangers. AIP Conf Proc 2008;985(1):606–13.

[33] Ardhapurkar PM, Sridharan A, Atrey MD. Flow boiling heat transfer coefficients at cryogenic temperatures for multi-component refrigerant mixtures of nitrogen–hydrocarbons. Cryogenics 2014:5984–92.

[34] Silver L. Gas cooling with aqueous condensation. Trans Inst Chem Eng 1947:2530–42.

[35] Bell KJ, Ghaly MA. An approximate generalized design method for multicomponent/partial condenser. AIChE Symp Ser 1973;69(131):72–9.

[36] Granryd E. Heat transfer in flow evaporation of non-azeotropic refrigerant mixtures – a theoretical approach. In: Proc 18th int congress of refrigeration. montreal; 1991. p. 1330–4.

[37] Tu X, Hrnjak P. Flow and heat transfer in microchannels 30 to 300 microns in hydraulic diameter. Air Conditioning and Refrigeration Center. College of Engineering. University of Illinois at Urbana–Champaign; 2004.

[38] Qu W, Mudawar I. Flow boiling heat transfer in two-phase micro-channel heat sinks––I. Experimental investigation and assessment of correlation methods. Int J Heat Mass Transf 2003;46(15):2755–71.

[39] Li M, Dang C, Hihara E. Flow boiling heat transfer of HFO1234yf and HFC32 refrigerant mixtures in a smooth horizontal tube: Part II. Prediction method. Int J Heat Mass Transf 2013;64:591–608.